Faraday Discuss., 1994, **97**, 401–413

Solvation and Vibrational Effects on Proton Tunnelling in Clusters

Jack A. Syage
The Aerospace Corporation, P.O. Box 92957/M5-754, Los Angeles, CA 90009, USA

Recent experiments indicate that excited-state proton transfer in $ROH(NH_3)_n$ clusters (where ROH is 1-naphthol or phenol) occurs by a tunnelling mechanism. A theoretical framework for describing the role of solvent and vibrations on proton tunnelling rates is discussed. Two previous models of proton tunnelling in clusters are examined; one based on a solvent-independent bound–continuum potential and the other on a solvent-activated bound–bound potential. In this work we extend the latter model to incorporate coupling of the proton to reactant and product vibrations. All three models are compared to experimental tunnelling rates in clusters and their attributes discussed.

Clusters are important for studying properties of the bulk on an atomic or molecular level and for understanding departures from bulk-phase behaviour as the system size approaches the single-molecule gas-phase limit. Our work centres on the study of chemical reactivity in clusters using time-domain techniques. The questions we are trying to address include: (1) how do individual solvent molecules contribute to energetics and dynamics of chemistry; (2) what solvent motions and intermolecular vibrations facilitate reactions; and (3) what kind of theories are needed to describe dynamical processes in clusters? An important question to ask is what information can small clusters provide that is unattainable in condensed-phase studies? The short answer is they offer the potential to (1) achieve isoenergetic excitation without thermal averaging, (2) measure effects due to specific solvent configurations or at least cluster size, (3) perform more exacting calculations due to the manageable number of molecules involved.

These discussions will focus on excited-state proton transfer reactions (ESPT) of the form

$$ROH^*\cdots B_n \xrightarrow[k]{} [RO^{*-}\cdots H^+B_n]_{uc} \xrightarrow[k_s]{} [RO^{*-}\cdots H^+B_n]_{rc}$$

where ROH is an aromatic acid (*e.g.*, 1- and 2-naphthol and phenol), B is a base-type solvent molecule, and n is the number of solvent molecules in the cluster. We assume a two-step process involving initial proton transfer followed by solvent reorganization from an unrelaxed (uc) to a relaxed (rc) configuration. Owing to the growing number of studies, ESPT in clusters is developing into a prototype for evaluating the role of individual solvent molecules on chemical reactivity. Leutwyler and co-workers pioneered the study of ESPT in clusters in a series of experiments on 1- and 2-naphthol (NpOH) that revealed distinct threshold size dependences that varied with solvent proton affinity.[1,2] Tramer *et al.* reported threshold behaviour for phenol (PhOH) by measuring changes in ionization potential with n.[3] These seminal studies provided valuable spectroscopic data and details regarding the thermochemistry of ESPT. Picosecond time-resolved measurements were conducted by Zewail and co-workers for 1-NpOH,[4] by Bernstein and co-workers for protio and deuterio 1-NpOH,[5] and by Steadman and Syage for protio and

deuterio PhOH.[6–10] These studies were conducted for a variety of solvents and rates were measured as a function of n by resonance ionization mass spectrometry. Knochenmuss *et al.*[11] measured ESPT in 1-NpOH$(H_2O)_n$ by picosecond fluorescence spectroscopy for medium to large clusters and Hineman *et al.*[12] reported on fragmentation in PhOH$(NH_3)_n$ using picosecond multiphoton ionization. ESPT involving aromatic acids has been studied extensively in the condensed phase including several time-resolved experiments,[13–15] which gives a valuable base of information for comparing to cluster results.

In the following we present a discussion on the dynamics of tunnelling. An attempt is made to frame the subject in the context of condensed-phase tunnelling theory. We will discover, though, that small clusters do not behave as bulk solvent, but neither do they follow gas-phase behaviour. To bridge this gap we propose a model for incorporating solvent vibrational interactions.[16–18] The intent of this work is to open discussion on how to model reactivity and solvation in small clusters.

Background

In a typical experiment, a molecular beam of clusters is photoexcited to a reactive state by a pump pulse and the evolution of some property (*e.g.*, relaxation, spectral shifts, or reactant decay and product formation) is monitored by a variably delayed probe pulse using multiphoton ionization. The majority of our experiments use time-of-flight mass spectrometry to measure dynamics as a function of cluster size.[6–10,19,20] Recently, we applied time-resolved photoelectron spectroscopy (TRPES) to the measure of dynamical properties in clusters.[10,21] Details of the experiments can be found in the original papers and review articles.

The driving force behind ESPT is the proton affinity of the solvent cluster. The simplest view is that RO^{*-} and B_n compete for the proton and that the reaction Gibbs energy $\Delta G_{0,n}$ depends on the proton affinity of these two moieties. Thermochemical cycles, based on this principal, have proved useful for describing the qualitative dependence of reactivity on properties of the solvent B_n. Some attempts have been made to include other interactions (*e.g.*, Coulombic interactions)[6] and to model the potential-energy surface along a few relevant coordinates (*e.g.*, O—H and solvent coordinate),[9] but rigorous theoretical calculations of the reaction energetics are lacking. Nonetheless, experimental results have clarified many properties of ESPT in clusters. Some important conclusions are as follows:

(1) The solvent proton affinity increases in fairly large discrete steps for the addition of the first few solvent molecules (and $\Delta G_{0,n}$ decreases in a similar stepwise manner). As the cluster grows in size, the steps become smaller and proton affinity converges to the bulk-phase limit (basicity). For strong base molecules where reaction occurs for small n (*e.g.* NH_3) a change from positive to negative Gibbs energy can occur by addition of a single solvent molecule. This explains the sharp size thresholds for ESPT observed for many systems.[1–8] An example of this effect is given in Fig. 1, which shows in the time-domain that photoexcitation of PhOH$(NH_3)_n$ leads to a distinct onset of reaction at $n = 5$.[6,20] Similar measurements on 1-NpOH$(NH_3)_n$ show an onset at $n = 3$ reflecting the greater acidity of 1-NpOH relative to PhOH.[4,5]

(2) ESPT rates increase gradually with excess energy in 1-NpOH$(NH_3)_n$ indicating a barrier process.[5] A time constant of about 60 ps of PhOH$(NH_3)_n$ at 2500 cm^{-1} of excess energy also suggests a barrier impedance to reaction.[6] A model of the potential energies indicates that the proton transfer state derives from a high-lying charge-transfer state of phenol. The stabilization of this state by successive addition of solvent molecules is shown in Fig. 1.

(3) A strong proton/deuteron isotope effect on rates for 1-NpOH[5] and PhOH[9] in $(NH_3)_n$ solvent clusters indicates that proton transfer occurs by tunnelling. For example,

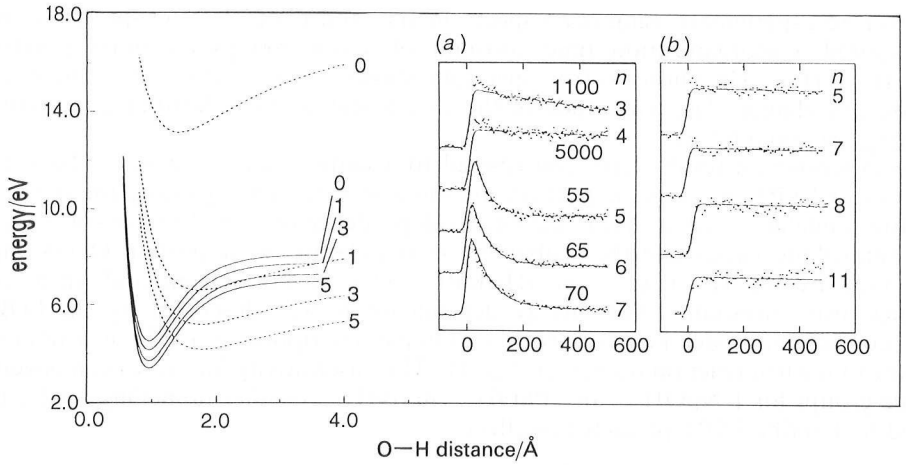

Fig. 1 Approximate $PhOH(NH_3)_n$ cluster potential-energy curves for the reactive PhO–H coordinate. These curves assume an equilibrium O···N bond distance (*ca.* 1.8 Å and 1.0 Å for the neutral and ion-pair states, respectively). Insert shows observed lifetime/ps of the reactant $PhOH^*B_n$ (as measured by $PhOH^+B_n$ detection) in solvent clusters (*a*) $(NH_3)_n$ and (*b*) $(CH_3OH)_n$ at 2500 cm^{-1} internal energy. The calculated curves are described in ref. 6 and 20. Calculated curves for the $(CH_3OH)_n$ data assume a 10 ns lifetime.

ESPT lifetimes for $C_6H_5OD(ND_3)_n$ and $C_6D_5OD(ND_3)_n$ range from 1 to 2.5 ns for $n = 5$ and 6 *versus* about 60 ps for $C_6H_5OH(NH_3)_n$.[9] The observation of ESPT from the vibrationless levels of 1-$NpOH(NH_3)_n$ also supports a tunnelling mechanism.[4,5]

(4) The proton is strongly coupled to product and solvent vibrational modes as evidenced by a large structural change that occurs after proton transfer. In separate

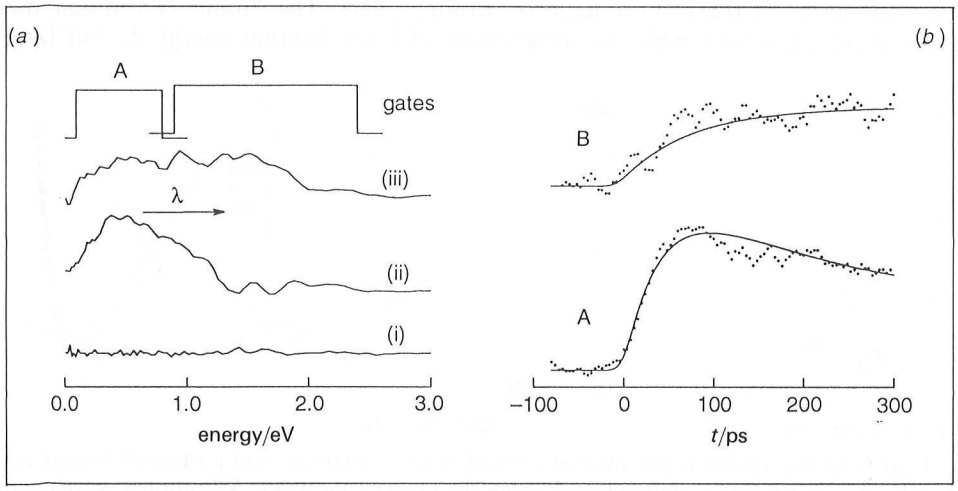

Fig. 2 Time-resolved photoelectron spectra as a function of pump-probe delay time *t*. (*a*) Difference spectra corresponding to (pump + probe) − (pump). Delay times are: (i) −100, (ii) +100 and (iii) +400 ps. (*b*) Observed time-dependences of the low-energy (gate A) and high-energy (gate B) photoelectron bands are plotted. Fitted curves were calculated for rate constants $k = (50\ ps)^{-1}$ and $k_s = (300\ ps)^{-1}$ and spectral parameters discussed in ref. 10.

time-resolved experiments using mass spectrometry[6] and photoelectron spectroscopy,[10] we measured a reorganization time constant of about 300 ps for initially formed $PhO^{*-}H^{+}(NH_3)_n$. The photoelectron spectrum, shown in Fig. 2, evolved in time due to the geometry change. The magnitude of the shift is significant indicating a reorganization energy of about 0.5 eV.

The experimental results have contributed to a better understanding of the barrier properties of ESPT, however, important questions still remain regarding the dynamics of proton tunnelling, such as: (1) Is the energy dependence of k attributable solely to the O—H tunnelling barrier and the probability of populating the important O···N mode as assumed by the Hineman *et al.* (HBKB) model, or are solvent and vibrational dynamics also important? The energy dependence is well described by the HBKB bound–continuum model, however, is this a unique description? (2) Why is k relatively invariant to n when reaction occurs (*cf.* Fig. 1)? This insensitivity has now been observed by three groups for 1-NpOH[4,5] and PhOH[6,9] in $(NH_3)_n$. Neither tunnelling model thus far used to describe ESPT predicts this effect.

Barrier Models

In previous work we showed that the ion-pair product potential derives from a charge-transfer or ion-pair state of isolated phenol that corresponds to the dissociative limit $PhO^{*-} + H^{+}$.[6,20] This state is stabilized significantly by molecules with high proton affinity as shown by the energy diagram in Fig. 1. This simple picture predicts a surface crossing along the O—H coordinate with the initially excited S_1 Coulombic state of phenol. It also predicts that ESPT becomes exoergic for some minimum, but small, number of NH_3 molecules. The simple model is intuitive, but neglects other stabilizing interactions, which explains why the predicted and observed onset values of n differ.

Two conceptually different models have been used lately to describe proton tunnelling in clusters; the first developed by Hineman *et al.* (HBKB)[5] is based on a bound-to-continuum proton transition [Fig. 3(*a*)] and the second proposed by us is based on a bound-to-bound proton transition [Fig. 3(*b*)] mediated by solvent motion (condensed-phase picture).[9] Both models use Bell theory for the tunnelling interaction[22] and obtain good predictions of the proton/deuteron isotope effect. The bound–continuum model obtains good agreement with the dependence of k on internal energy E, but fails to

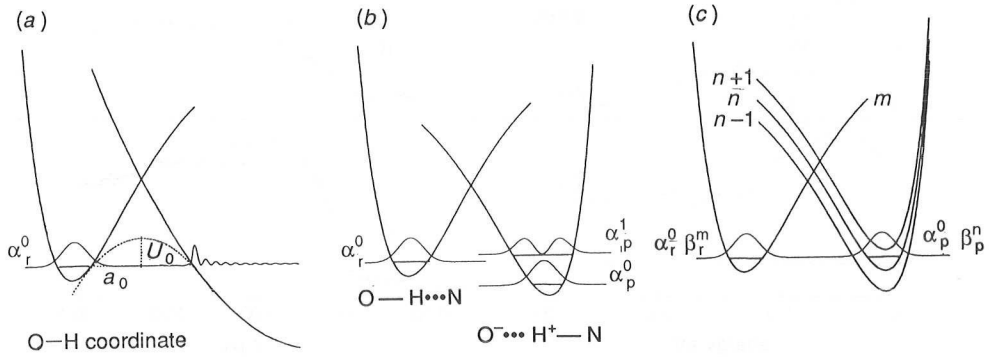

Fig. 3 (*a*) Bound–continuum potential, (*b*) bound–bound potential, and (*c*) bound–bound potential with vibrational energy shifts plotted along the O—H coordinate. Vibrational wavefunctions for the O—H oscillator are denoted by α where the subscripts r and p refer to reactant and product, and the superscript denotes number of quanta. β_r^m and β_p^n refer to a reactant (m quanta) and product (n quanta) vibration that couples to proton translocation. Non-adiabatic curves are shown. An inverted parabolic barrier (avoided crossing) of height U_0 and halfwidth a_0 is used for calculations.

describe the dependence of k on cluster size (*i.e.* reaction Gibbs energy ΔG_0). The solvent-activated bound–bound model obtains only fair agreement on E and ΔG_0. The difference between the two models is in how they treat the density of product states coupled to the reactive O—H coordinate. The former model is simplistic in assuming a continuum of product states [Fig. 3(*a*)] and, therefore, suffers from too broad a density of states. The latter model [Fig. 3(*b*)], though fundamentally more realistic, suffers from too narrow a density of states by assuming coupling to only the vibrationless N—H stretch mode of the product. In real systems one expects many vibrations in the product to couple to the proton, the effect of which is to broaden the density of accepting states to an extent determined by Franck–Condon relations. This possibility is illustrated by the barrier picture in Fig. 3(*c*).

A minimum of four nuclear coordinates are needed to discuss proton tunnelling properly: (1) the O—H coordinate q_H, which is the reaction coordinate; (2) the O···N coordinate Q_N, in which the O···N symmetric stretch modulates the internuclear distance between potential minima, which in turn modulates the barrier height and width; (3) the solvent coordinate S, in which solvent modes cause fluctuations in the relative energies of reactant and product; and (4) coordinates corresponding to product accepting modes that reduce the energy gap between reactant and product. All coordinates, except S, are treated quantally. We begin in Fig. 3(*b*) with a schematic representation of the bound Coulombic and ion-pair potentials along the O—H coordinate for a fixed O···N and solvent coordinate. The example given in Fig. 3(*b*) is for an asymmetric double well (*i.e.* different minima energy). Vibrational probability functions are drawn for the O—H and N—H vibrationless levels of the reactant and product, α_r^0 and α_p^0, respectively, and for the $v = 1$ level of the product α_p^1. For the asymmetric potential the vibrational wavefunctions are localized in either well with miniscule probability leaking into the other well. In this case the tunnelling probability is insignificant.

Condensed-phase theories of proton tunnelling, such as those of Borgis and Hynes,[16] and Cukier and Morillo,[17] assume that tunnelling occurs when the solvent (through thermal fluctuations) achieves critical but momentary configurations for which the potential wells become symmetric. Under these conditions where the zeroth-order vibrational energies are degenerate, the tunnelling interaction is strongest (*i.e.* tunnelling splitting) and the vibrational probabilities become delocalized over both potentials. In other words, the tunnelling probability is maximized. A similar tunnelling enhancement would occur if the α_r^0 and α_p^1 zeroth-order states became degenerate. The concept of solvent fluctuations creating momentary symmetric potentials is based on Marcus theory of electron transfer.[23,24]

The critical solvent configurations $S^\ddagger$ for achieving the symmetric potential for tunnelling will most likely be different from the equilibrium solvent geometries of the reactant and product states, S_r and S_p, respectively. Schematic representations of the O—H potential for S_r and S_p are given in Fig. 4A. This picture is important because it implies that the solvent must move for an exoergic reaction to proceed. Plotting reactant and product minima energies as a function of solvent coordinate in Fig. 4B indicates that there is an activated solvent configuration $S^\ddagger$ at energy $\Delta G^\ddagger$ for bringing the reactant and product minimum energies (or vibrationless levels) into resonance for tunnelling. The difference in the energy of the product for the solvent geometries S_r and S_p is sometimes referred to as the solvent reorganization energy λ_S, and is a quantity we measure by time-resolved photoelectron spectroscopy.[6]

According to Fig. 3(*b*), large solvent fluctuations are necessary to achieve tunnelling resonances because of the large energy gap between reactant and product. This leads to predicted temperature dependences that are much steeper than observed in bulk and in clusters and to a predicted slowing of tunnelling rates for large exoergicities (*i.e.*, Marcus inverted region) that are rarely observed. The problem is circumvented by considering other vibrations β that couple to the O—H coordinate (*e.g.*, O···N stretch and solvent–

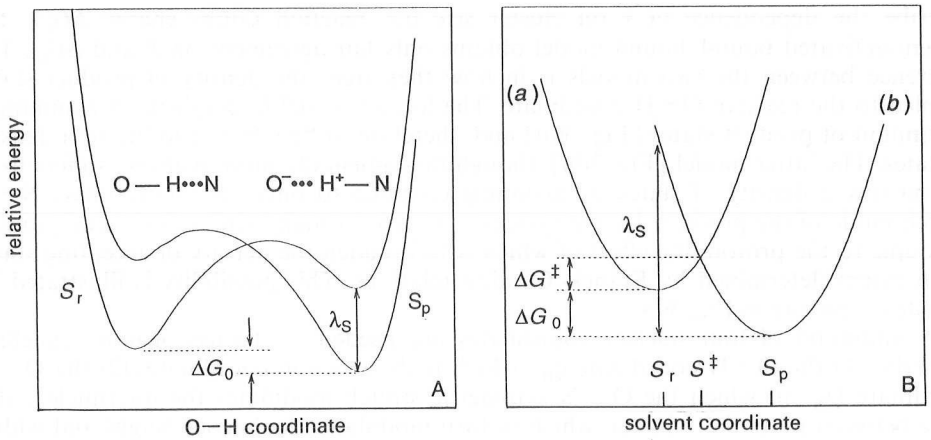

Fig. 4 A, Schematic representation of the potential energy along the O—H coordinate for fixed solvent configurations S_r and S_p. B, Reactant (*a*) and product (*b*) minimum energy as a function of solvent coordinate S. $\Delta G^\ddagger$ is the free energy of activation for achieving resonance between the reactant and product minimum (vibrationless) energy. ΔG_0 is the free energy of reaction for an equilibrating solvent. λ_S is the solvent reorganization energy.

solvent bending modes) to reduce energy gaps between reactant (r) and product (p) as depicted in Fig. 3(*c*) by the combination states $\alpha_r^0\beta_r^m$ and $\alpha_p^0\beta_p^n$. A similar series of product curves should be envisioned for Fig. 4A and B. In reality a quasicontinuum of states may exist to provide additional bridging of energy gaps between reactant and product. Modelling the vibrational manifold is important because the smaller the reaction energy gap, the less important is solvent motion for bringing reactant and product into resonance.

Tunnelling Models

A detailed discussion comparing bound–continuum and solvent-activated bound–bound proton tunnelling can be found in ref. 9. We reiterate essential features and then show how vibrations are incorporated into the latter model. The two models of tunnelling can be compared by the following rate equations

$$W_{r\to p} = \nu_H \exp[-2\Omega] \qquad \text{(bound–continuum transition)} \tag{1}$$

$$W_{r\to p} = \frac{h\nu_H^2}{2}\exp[-2\Omega]\left(\frac{\beta}{\pi\lambda_S}\right)^{1/2}\exp[-\beta\Delta G^\ddagger]$$

$$\text{(solvent-activated bound–bound transition)} \tag{2}$$

where ν_H is the O—H vibrational frequency and

$$\Omega = \frac{\pi^2 a}{h}(2mU)^{1/2} \tag{3a}$$

$$\Delta G^\ddagger = (\Delta G_0 + \lambda_S)^2/4\lambda_S \tag{3b}$$

$$\beta^{-1} = (k_B T + E_{vib}/s) \tag{3c}$$

The terms in Ω and $\Delta G^\ddagger$ are defined in Fig. 3 and 4. T is the initial cluster temperature (k_B is the Boltzmann constant), E_{vib} is the vibrational excitation energy in S_1, and s is the number of effective degrees of freedom in the cluster that contribute to the heat capacity. β^{-1} is loosely defined as an energy per effective degree of freedom. (We use linear not angular frequency units throughout, *i.e.* s^{-1}.)

It is useful to cast the above equations as Golden Rule type equations of the form

$$W_{r\to p} = \frac{4\pi^2}{h} C^2 \rho \tag{4}$$

in order to separate the terms associated with the coupling C and the effective density of states ρ. The tunnelling splitting for an O—H symmetric double-well potential with an inverted parabolic barrier is given by[22]

$$2C = \frac{h\nu_H}{\pi} \exp[-\Omega] \tag{5}$$

Using eqn. (4) and (5) it is possible to sort out the terms in eqn. (1) and (2) that correspond to an effective density of states as follows:

$$\rho = \frac{1}{h\nu_H} \qquad \text{(bound–continuum transition)} \tag{6}$$

$$\rho = \frac{1}{2}\left(\frac{\beta}{\pi\lambda_S}\right)^{1/2} \exp(-\beta\Delta G^{\ddagger}) \quad \text{(bound–bound transition)} \tag{7}$$

The reaction Gibbs energy ΔG_0 is the driving force for proton transfer. Eqn. (7) is identical to that obtained from the classical Marcus theory of electron transfer.[23] The dependence of ρ on ΔG_0 is vastly different by the two models; it is a constant value for the bound–continuum case and a strongly peaked function about the value λ_S for the bound–bound case. The latter case is plotted in Fig. 5(*a*) for different internal energies β^{-1}. Since W is directly proportional to ρ, Fig. 5(*a*) predicts a rate that peaks at $\Delta G_0 = -\lambda_S$ and then decreases with increasing exoergicity. This behaviour is the so-called Marcus inverted region. A second outcome of the peaked density function is a potentially large temperature dependence. Oddly, the temperature dependence becomes negative as $-\Delta G_0/\lambda_S$ approaches unity. For comparison, the value of ρ by eqn. (6) is indicated in Fig. 5 by the arrow.

The peculiar behaviour predicted by eqn. (7) (and classical Marcus theory of electron transfer) is generally moderated in real systems by the coupling of the proton to vibrational modes other than O—H and N—H as depicted by the coupling of the reactant potential to a manifold of product potentials in Fig. 3(*c*). Coupling refers to vibrations that undergo changes in quantum number due to proton transfer [*e.g.* mode β in Fig. 3(*c*)].[23–25] Eqn. (7) is then modified to include a sum over a Franck–Condon probability distribution for change in quantum number, *i.e.*

$$\rho_{\{m\}} = \frac{1}{2}\left(\frac{\beta}{\pi\lambda_S}\right)^{1/2} \sum_{n_1=0}^{\infty} \cdots \sum_{n_M=0}^{\infty} \prod_{i}^{M} |\langle m_i | n_i\rangle|^2 \exp[-\beta\Delta G^{\ddagger}_{m_i,\,n_i}] \tag{8}$$

(vibrational and solvent-activated tunnelling)

where M is the number of coupled modes and

$$\Delta G^{\ddagger}_{m_i n_i} = \frac{1}{4\lambda_S}\left[\Delta G_0 + \lambda_S + \sum_i (n_i - m_i)h\nu_i\right]^2 \tag{9a}$$

$$|\langle m | n\rangle|^2 = m!n! \exp(-Z)\left|\sum_{q=0}^{\min(m,n)} (-1)^{n-q} \frac{Z^{(m+n-2q)/2}}{q!(m-q)!(n-q)!}\right|^2 \tag{9b}$$

$$Z_i = \lambda_i/h\nu_i \tag{9c}$$

[we have dropped the subscript i in eqn. (9*b*) for clarity]. The function $\rho_{\{m\}}$ is defined as the effective density of product states coupled to reactant state $\prod_i |m_i\rangle$. Eqn. (9*b*)

ground section, the observation that k is relatively insensitive to n and ΔG_0 for 1-$NpOH(NH_3)_n$ and $PhOH(NH_3)_n$ was unexpected and at first difficult to explain. The bound–continuum model predicts an exponentially increasing k with ΔG_0 because the effect of changing ΔG_0 is due solely to the change in the tunnelling barrier parameters U_0 and a_0. In the activated-solvent models an additional dependence on ΔG_0 appears in the solvent activation energy $\Delta G^{\ddagger}$. However, in the absence of product vibrational coupling, the dependence is exaggerated [Fig. 5(*a*) and 7]. With vibrational coupling added to the model, the effect is moderated [Fig. 5(*b*) and 7] and more realistic. In this example, we used a single-mode treatment involving only ν_N.

To summarize, the bound–continuum model is able to describe well the dependence on internal energy E, but not on ΔG_0. The bound–bound activated-solvent model has an excessive sensitivity to some parameters that can lead to predictions of extreme dependences on E and ΔG_0 in certain situations, although the model contains the necessary features to describe the ΔG_0 dependence. The inclusion of vibrational coupling moderates the harshness of the activated solvent model. It should be noted that a simple single-mode calculation using just the O···N promoting and accepting mode, as applied in Fig. 7, was able to give nearly as a good a description of experimental dependences as the multimode approach. A better method of treating vibrations should be explored once experimental measurements of important vibrational parameters become available. A number of other issues are left open: (1) the use of a Boltzmann factor for the solvent-activation is not strictly correct for the isoenergetic excitation of clusters; (2) the classical solvent coordinate is not valid in the limit of $E \rightarrow 0$; (3) the distinction between classical solvent modes and the low-frequency quantal modes is not made sufficiently clear; and (4) the dependence of the tunnelling barrier properties on ΔG_0 is uncertain. This work would probably benefit from an effort to replace the classical solvent treatment leading to a Boltzmann expression with a semiclassical approach that considers a statistical probability of populating critical solvent modes. Further experimental and theoretical work is needed to bridge our understanding of chemical dynamics from clusters to the condensed phase.

References

1 O. Cheshnovsky and S. Leutwyler, *Chem. Phys. Lett.*, 1985, **121**, 1; O. Cheshnovsky and S. Leutwyler, *J. Chem. Phys.*, 1988, **88**, 4127.
2 R. Knochenmuss and S. Leutwyler, *J. Chem. Phys.*, 1989, **91**, 1268; T. Droz, R. Knochenmuss and S. Leutwyler, *J. Chem. Phys.*, 1990, **93**, 4520.
3 D. Solgadi, C. Jouvet and A. Tramer, *J. Phys. Chem.*, 1988, **92**, 3313; C. Jouvet, C. Lardeux-Dedonder, M. Richard-Viard, D. Solgadi and A. Tramer, *J. Phys. Chem.*, 1990, **94**, 5041.
4 J. J. Breen, L. W. Peng, D. M. Willberg, A. Heikal, P. Cong and A. H. Zewail, *J. Chem. Phys.*, 1990, **92**, 805.
5 M. F. Hineman, G. A. Bruker, D. F. Kelley and E. R. Bernstein, *J. Chem. Phys.*, 1992, **97**, 3341.
6 J. Steadman and J. A. Syage, *J. Chem. Phys.*, 1990, **92**, 4630; J. A. Syage and J. Steadman, *J. Chem. Phys.*, 1991, **95**, 2497.
7 J. Steadman and J. A. Syage, *J. Am. Chem. Soc.*, 1991, **113**, 6786; J. A. Syage and J. Steadman, *J. Phys. Chem.*, 1992, **96**, 9606.
8 J. Steadman and J. A. Syage, *J. Phys. Chem.*, 1991, **95**, 10326.
9 J. A. Syage, *J. Phys. Chem.*, 1993, **97**, 12523.
10 J. A. Syage, *Chem. Phys. Lett.*, 1993, **202**, 227; J. A. Syage, *Z. Phys. D.*, 1994, in the press.
11 R. Knochenmuss, G. R. Holtom and D. Ray, *Chem. Phys. Lett.*, 1993, **215**, 188.
12 M. F. Hineman, D. F. Kelley and E. R. Bernstein, *J. Chem. Phys.*, 1993, **99**, 533.
13 E. M. Kosower and D. H. Huppert, *Annu. Rev. Phys, Chem.*, 1986, **37**, 127.
14 J. Lee, R. D. Griffin and G. W. Robinson, *J. Chem. Phys.*, 1985, **82**, 4920; J. Lee, G. W. Robinson, S. P. Webb, L. A. Philips and J. H. Clark, *J. Am. Chem. Soc.*, 1986, **108**, 6538.
15 D. H. Huppert, A. Jayaraman, R. G. Maines, D. W. Steyert and P. M. Rentzepis, *J. Chem. Phys.*, 1984, **81**, 5596.
16 D. C. Borgis, S. Lee, and J. T. Hynes, *Chem. Phys. Lett.*, 1989, **162**, 19; D. C. Borgis and J. T. Hynes, *Chem. Phys.*, 1993, **170**, 315; D. C. Borgis and J. T. Hynes, *J. Chem. Phys.*, 1991, **94**, 3619.

17 R. I. Cukier and M. Morillo, *J. Chem. Phys.*, 1990, **91**, 857; M. Morillo and R. I. Cukier, *J. Chem. Phys.*, 1990, **92**, 4833.
18 P. F. Barbara, G. C. Walker and T. P. Smith, *Science*, 1992, **256**, 975.
19 J. A. Syage and J. Steadman, *Chem. Phys. Lett.*, 1990, **166**, 159; J. Steadman, E. W. Fournier and J. A. Syage, *Appl. Opt.* 1990, **29**, 4962.
20 J. A. Syage, in *Ultrafast Spectroscopy in Chemical Systems*, ed. J. D. Simon, Kluwer Academic Publishers, New York, 1993, p. 289; J. A. Syage, in *Femtosecond Chemistry*, J. Manz and L. Wöste, VCH Publishers, New York, 1994.
21 J. Steadman and J. A. Syage, *Rev. Sci. Instrum.*, 1993, **64**, 3094.
22 R. P. Bell, *The Tunnel Effect in Chemistry*, Chapman-Hall, New York, 1980, ch. 2.
23 R. A. Marcus, *Faraday Discuss. Chem. Soc.*, 1982, **74**, 7.
24 G. L. Closs and J. R. Miller, *Science*, 1988, **240**, 440.
25 J. Jortner and M. Bixon, *J. Chem. Phys.*, 1988, **88**, 167; J. Ulstrup and J. Jortner, *J. Chem. Phys.*, 1975, **63**, 4358; K. F. Freed, *Acc. Chem. Res.*, 1978, **11**, 74.
26 P. J. and K. A. Holbrook, *Unimolecular Reactions*, Wiley, New York, 1972.
27 S. Wei, W. B. Tzeng and A. W. Castleman Jr., *J. Phys. Chem.*, 1991, **95**, 585.

Paper 4/00103F; *Received 7th January*, 1994